Longitudinal Direct Ionization Impact of Heavy Ions on See Testing for Ultrahigh Energies

Vanessa Wyrwoll, Rubén García Alía, Ketil Røed, Carlo Cazzaniga, Maria Kastriotou, Pablo Fernández-Martínez, Andrea Coronetti, and Francesco Cerutti

***Abstract*— Ultrahigh-energy (UHE) heavy ions show various advantages at testing single-event effect (SEE) in modern technologies, due to their highly penetrating nature. However, the intercepting material in the beam line contributes to the modification of the beam structure by generation of fragments produced via nuclear interactions. This is especially relevant for UHE heavy ion beams, representative of energies in space, which are not fully investigated through conventional ground-level testing. This article is dedicated to the study of the longitudinal energy deposition mechanisms in silicon by the aforementioned heavy ion beams and their fragments. The presented studies have been carried out using Monte Carlo simulations triggered by experimentally observed phenomena.**

***Index Terms*— CERN, FLUKA, Monte Carlo simulation, single-event effects (SEEs).**

I. Introduction

ELECTRONIC testing is carried out in many ways utilizing the modern available facilities. Depending on the aim of the single-event effect (SEE) tests, an adequate beam must be chosen. For space application SEE tests, a broad range of heavy ions of 10 MeV/n are available at the RADiation Effects Facility in Finland (RADEF) [1] and at the Centre de Recherches du Cyclotron, Université Catholique de Louvain-la-Neuve, Belgium (UCL) [2]. Facilities such as Texas A&M University (TAMU) [3], Berkeley Accelerator Space Effects (BASE) [4], Kernfysisch Versneller Instituut (KVI) [5], and Grand Accélérateur National d'Ions Lourds (GANIL) [6], for instance, offer a higher energy range between 10 and 100 MeV per nucleon. Gesellschaft für Schwerionenforschung (GSI) [7] or NASA Space Radiation Laboratory (NSRL) [8] provide energies from 100 MeV/n up to 5 GeV/n. Going up even higher in terms of particle energy, CERN has recently provided opportunities for performing ultrahigh energy (UHE) heavy ion tests up to several hundred GeV/n.

Manuscript received April 24, 2020; revised April 30, 2020 and May 5, 2020; accepted May 8, 2020. Date of publication May 14, 2020; date of current version July 16, 2020. This work was supported by the RADiation and reliability challenges for electronics used in Space, Avionics, on the Ground and at Accelerators (RADSAGA) funding from the European Union's Horizon 2020 Research and Innovation Program under Grant 721624.

Vanessa Wyrwoll, Rubén García Alía, Maria Kastriotou, Pablo Fernández-Martínez, Andrea Coronetti, and Francesco Cerutti are with CERN, 1211 Genève, Switzerland (e-mail: vanessa.wyrwoll@cern.ch).

Ketil Røed is with the Department of Physics, University of Oslo, 0315 Oslo, Norway.

Carlo Cazzaniga is with the ISIS Facility, Science and Technology Facilities Council, Rutherford Appleton Laboratory, Didcot OX11 0QX, U.K.

Color versions of one or more of the figures in this article are available online at http://ieeexplore.ieee.org.

Digital Object Identifier 10.1109/TNS.2020.2994370

In addition to heavy ions of various energies, 200 MeV protons are widely used, e.g., at the Paul Scherrer Institute (PSI) [9], which represents like RADEF and UCL, an European Space Agency (ESA)-supported facility. Energetic ions are of special interest, since the radiation environment in space, focusing on the galactic cosmic-ray (GCR) spectrum, consists of heavy ions with energies mainly extending up to the UHE regime, defined as 5–150 GeV/n in [10]–[12].

For SEE testing with heavy ions, the linear energy transfer (LET) is the main figure of merit. The cross section from direct ionization, which is the main mechanism for heavy ions, can vary significantly with the LET. Hence, it is important to retrieve the LET threshold and the saturated cross section. Typically, the LET can be varied between 1 and 60 MeV cm^2/mg for standard energies and ions. Thus, testing with various LETs in standard facilities can cover for the particles commonly found in the space environment. First, the SEE cross section as a function of LET is retrieved in tests through variation of ions and energies. Then, convolving this function with the environmental LET curve of the GCR spectrum leads to the expected SEE rate [13].

However, because GCR consists of ions reaching their maximum flux at energies between 500 MeV/n and 1 GeV/n energies [13], which are not easily available in conventional ground-level facilities with standard energies around 10 MeV/n, it is important to investigate possible ion energy effects which may be missed by restricting the analysis to the sole LET compatibility.

Previous works have shown that the approach of relying on the LET and device dimensions might not be accurate enough [14] and more parameters play a role in the resulting upset number than the LET value of a particle, such as incident particle energy and species [15]–[17]. Moreover, a discrepancy has been observed, especially for low LET ions below the LET threshold, caused by nuclear interactions, which contribute to the SEE cross section of a device [18].

With this purpose, the interaction of UHE heavy ions with matter has been studied in [12]. This led to the definition of the volume-equivalent LET, which corresponds to the amount of energy deposited in a micrometer-scale structure divided by its thickness and material density (therefore, expressed in LET units). For standard ground-level ion test energies, the unrestricted (i.e., the one typically tabulated) and the volume-equivalent LET essentially coincide. However, for larger energies, the radial ionization structure is such that only a fraction of the energy is deposited in micrometer-scale SEE representative volumes, and, therefore, the volume-equivalent

LET is only a fraction of the total unrestricted value [11]. Furthermore, charge collection within the device is complex and impacted by the size of the sensitive volume (SV), as well as by the material surrounding it [19].

In our previous work, focused on UHE heavy ion beams available at CERN, the advantages and challenges of these beams have been discussed. García Alía *et al.* [12] focused on the radial ionization structure of UHE heavy ion beams, Fernández-Martínez *et al.* [11] discussed the experimental results and approaches for SEE testing in the specific beams available at CERN 2017 and 2018, whereas Kastriotou *et al.* [10] investigated the impact of beam composition of the mentioned beams. Furthermore, Criswell *et al.* [15] analyzed the occurring beam fragmentation in silicon and possible impact of SEEs caused by nuclear interaction in the sub-LET region.

This work focuses on the impact of the longitudinal (as opposed to radial) energy deposition distribution and thus on the actual LET for SEE testing. These tests are carried out in several facilities, such as RADEF in Finland, able to provide a cocktail of ions with energies of 9.3 MeV/n. Focusing on ions of this energy and their penetration capability, a range of 202 μm in silicon can be achieved by ^{15}N, whereas higher LET ions in this cocktail have much lower range (e.g., 89 μm for ^{131}Xe and 94 μm for ^{83}Kr) [20]. This parameter is of high importance since the ions need to be able to penetrate the device in the SV depth for at least 40 μm [21]. Thus, microelectronic parts typically need to be delidded of their package prior to irradiation. Furthermore, testing in vacuum is required to avoid energy loss through interaction of the ions with air. Unfortunately, opening modern state-of-the-art components is expensive and difficult to perform [12] or even impossible with some of the modern device structures [22]. These electronic components are smaller than in the past, more sensitive, and with increasingly complex structures [23]. All such complexities are removed when a UHE ion beam, for example, ^{208}Pb at 150 GeV/n [10]–[12], [17], is employed. Moreover, 3-D structures and stacked boards [10] can also be exposed to such a beam, as long as the beam does not experience high fragmentation and loss of intensity.

The physical phenomena featuring UHE beams must be fully understood for a proper interpretation of experimental findings. Material can be present in the beam line during the experiment, in the frame of beam shaping or beam analysis instrumentation. Particles at UHE energies are able to penetrate through matter without suffering a major energy loss and LET change. Hence, the physical mechanisms must be determined regarding the resulting energy deposition in the SV and potential fragmentation as soon as the material is inserted into the beam line.

Therefore, this article is focused on the UHE energy regime of heavy ions and their energy deposition characteristics in silicon. Experiments have been performed in a 150-GeV/n ^{208}Pb beam at CERN using a 140-μm silicon detector [24], [25]. Furthermore, the longitudinal distribution of the deposited energy and LET of heavy ions with very high energies (VHEs) from 100 MeV/n to 5 GeV/n and UHEs from 5 to 150 GeV/n [12] is studied via Monte Carlo simulations performed with FLUKA [26]. The impact of beam fragmentation is recovered by simulating the beam interaction with the air and with the beam-intercepting devices. The latter are reproduced as several layers of aluminum of various thicknesses.

II. Experimental Energy Deposition Distribution in a Silicon Detector

A. Facility Description

In the frame of the high-energy physics lead ion operation at CERN in November 2018, the Super Proton Synchrotron Experimental North Area (SPS-NA) served to irradiate several electronic devices with a 150-GeV/n ^{208}Pb beam. The beam was delivered in bunches of 8-s duration, with a periodicity of $\sim$45 s and intensities ranging from 10^3 to 10^5 ions per bunch, resulting in a flux between 10^2 and 10^4 ions/cm^2/s [10].

Dedicated instruments to monitor the beam, such as scintillators and a multiwire proportional chamber (MWPC), were installed in the beamline and served to guarantee a precise beam analysis in terms of field intensity and size. Besides, radiochromic film measurements were carried out in parallel during the irradiation as a cross calibration method.

B. Calibration of a Silicon Detector

The utilized setup in this article has been designed to avoid pileups and measure fast signals for high counting rate applications. For this, a 2 mm $\times$ 2 mm $\times$ 140 μm silicon detector was used to retrieve the experimental results presented. The diode is manufactured by Micron Semiconductors Ltd., with a fully depleted p-n-junction, a ceramic printed circuit board (PCB), and a metal housing. The experimental setup chain was as follows: A Cividec C2 low-noise current amplifier with an analog bandwidth of 2 GHz and a 40 dB gain, an ORTEC model 710 bias supply providing 40-V reverse bias voltage, and a CAEN digitizer processing the output signal in 1 GSamples per second–10 bits. The measurement has been performed in oscilloscope mode, which means that all waveforms triggering above a set threshold were recorded and analyzed offline according to their time stamps to generate energy histograms [27]. The calibration of the described setup has been performed in vacuum and the spectrum of the utilized triple-alpha source (Pu-239, Am-241, and Cm-244) can be seen in Fig. 1.

There the counts detected by the diode are illustrated over the corresponding alpha source energy. This correlation has been done by applying a calibration factor of 2.95 MeV per pulse area analyte-to-digital (ACD) counts times ns, as documented in more detail in the RADSAGA test report no. 7 [27].

C. Measurements of UHE Lead With a Silicon Detector

The tests discussed in this article were performed using a silicon detector with dimensions of 2 mm $\times$ 2 mm $\times$ 140 μm and a +20-dB preamplifier and −6-dB attenuators. An aluminum layer of roughly 20 μm, which was separated from the Si die by 0.5 cm of air, was present immediately in front of the detector to ensure that it was not exposed to light.

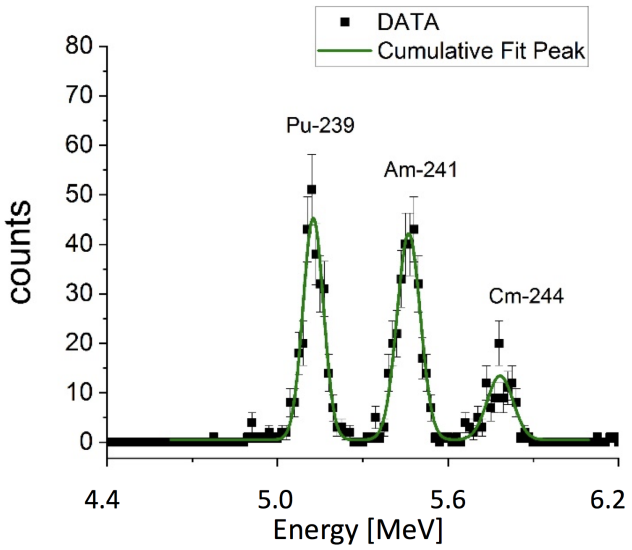

Fig. 1. Calibration spectrum of a 140-μm silicon detector retrieved in a triple-alpha source.

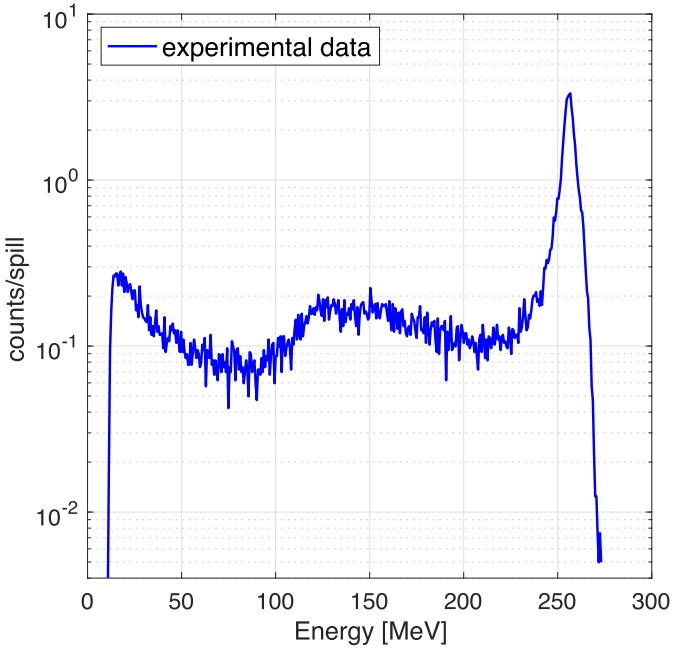

Fig. 2. Deposited energy spectrum of a 150-GeV/n ^{208}Pb beam in a 140-μm-thick silicon detector.

Fig. 2 shows the experimental energy deposition spectrum recorded with the described detector system in the SPS-NA 150-GeV/n ^{208}Pb beam. The total counts per spill as a function of the deposited energy show a clear distinguished direct ionization peak at 255 MeV, according to the calibration factor retrieved as explained above. Furthermore, a smaller peak can be observed in the low-energy end of the distribution, as well as an intermediate continuum between the two peaks.

III. Monte Carlo Simulations of Energy Deposition in a Silicon Detector

To investigate the impact of energy deposition events on electronic devices and the resulting SEEs, physical phenomena need to be studied. This can be done experimentally or numerically via Monte Carlo radiation transport techniques developed to solve such problems. These techniques can be divided into three categories [26]:

1) The developers have built the tool using established radiation transport physics.
2) The radiation toolkit designed for high-energy physics is utilized to design an application.
3) A precompiled Monte Carlo tool is used to develop an application.

Point three is the case for the Monte Carlo tool FLUKA [26], [28], [29]. As opposed to other Monte Carlo simulation codes, such as Geant4 or Monte Carlo Radiative Energy Deposition (MRED) [30], this article is based on FLUKA. Like Geant4 or MRED, FLUKA has been benchmarked extensively against experimental data [31], for instance, in terms of the fragmentation simulation by Fasso *et al.* [28] and Cerutti *et al.* [32].

In this work, FLUKA has been utilized to determine the physical processes involved in the fragmentation and direct ionization mechanisms. Since one of the most relevant aspects affecting this work is the nucleus–nucleus interaction model implemented within FLUKA, the work of Braun *et al.* [33] needs to be emphasized. There a fair agreement between FLUKA simulations and experimental data was observed. Under these conditions, a high accuracy and an error of under 5% in the maxima of the simulated energy deposition spectra presented in this article can be assumed.

Section III-A focuses on the energy deposition mechanisms in silicon when various materials are inserted in the beam line. Particle beams in the UHE regime are supposed to have a negligible energy loss while passing through material length characteristics of microelectronic devices [12]. Despite this, the simulation of the energy deposited via UHE beams can be done by applying a specific approach to simulate the event-by-event energy deposited in the SV. To perform such an event-by-event simulation, a special user routine structure has to be applied as described in [34]. In addition, different options must be chosen within a FLUKA input file, to enable or disable physical properties as needed for the research purpose under investigation. In the simulations described in this article, the physical phenomena have been mimicked in terms of nucleus–nucleus interactions for energies above 5 GeV/n by applying the Monte Carlo event generator Dual Parton Model and Jets (DPMJET III) [35]. This is especially important to get a realistic simulation of the beam fragmentation. Then, above 125 MeV/n and below 5 GeV/n, the mechanisms are physically described via the modified version of the relativistic quantum molecular dynamic (RQMD) code, now implemented in FLUKA as version RQM-2.4 [36]. Up to the energy of 125 MeV/n, nuclear interactions are described using the Boltzmann master equation (BME) [37]. Finally, for the fragmentation study part of this article, the electromagnetic dissociation was enabled in the input file, for both projectile and target ions. The simulations performed for this article have been done using the public FLUKA2011 Version 2x.6 Mar-2019.

A. Impact of Nuclear Fragmentation UHE Heavy Ion Beams

This section is dedicated to the energy deposition of UHE ^{208}Pb in a 140-μm silicon detector, representing the one tested experimentally and described in Section II. Moreover,

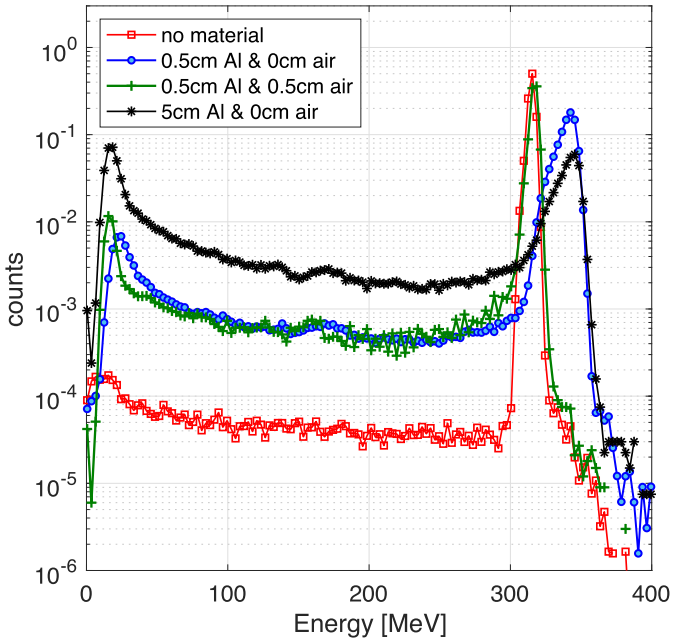

Fig. 3. FLUKA simulation of the energy deposition spectra in a 140-μm silicon detector for 150-GeV/n ^{208}Pb and increasing aluminum and air thicknesses in front of the SV.

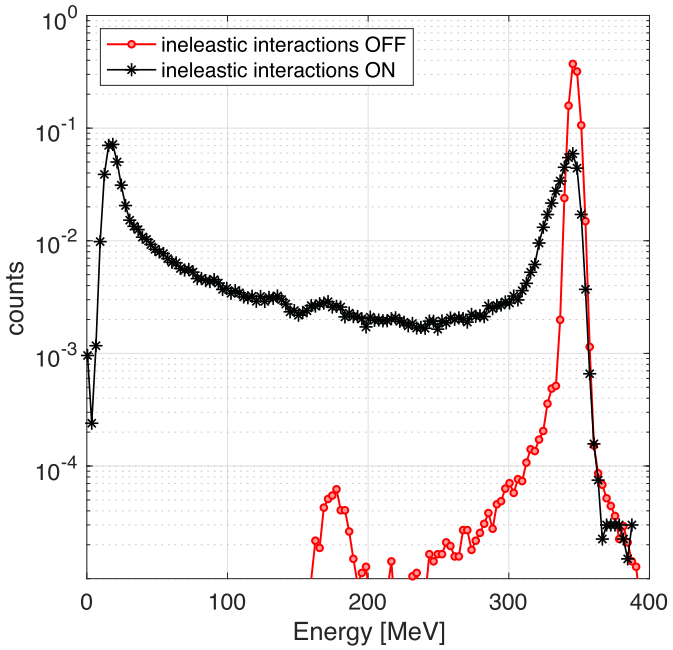

Fig. 4. FLUKA simulation of the energy deposition spectra in a 140-μm silicon detector for 150-GeV/n ^{208}Pb comparison between simulation including inelastic interaction and excluding them.

its interaction with different aluminum and air thicknesses is illustrated and discussed, with the purpose of mimicking the effect of the different beam instrumentation elements in the beamline.

A general comparison of the energy deposition spectra, implementing the mentioned beam characteristics, is illustrated in Fig. 3 for systematically increasing thickness of aluminum directly in front of the detector. The behavior is qualitatively similar to Fig. 2 for all curves: first, a minor peak at approximately 20 MeV, second a mid-part between 50 and 300 MeV, and third the distinguished ionization peak. A quantitative comparison is, however, not possible due to the lack of exact knowledge of the materials and thicknesses in the beamline during the experiments.

As a first step, the detector was simulated without any material in front of it. Then, an aluminum slab was introduced in the front, directly attached to the silicon. The thickness of aluminum was varied between 5 and 50 mm. It can be seen in Fig. 3 that aluminum thickness is directly proportional to the increase in intermediate energy deposition events. This is caused by very-high-energy inelastic fragments originated from nuclear interactions in aluminum depositing their energy in the SV, as further demonstrated in Fig. 4. There, again the energy deposition spectrum of a 150-GeV/n Pb beam is illustrated while 5 cm of aluminum is included in the beam line, directly attached to the diode's sensitive surface. The black curve shows the FLUKA simulation, as illustrated in Fig. 3 (in black), where all physics options are enabled and nothing is suppressed. As opposed to this, in the red curve, the inelastic interactions are turned off manually and are, therefore, not present in this simulation. As can be seen, the intermediate part almost disappears in the simulation, where the inelastic interactions are turned off. Hence, the increase in the intermediate part is caused by nuclear interactions/inelastic events.

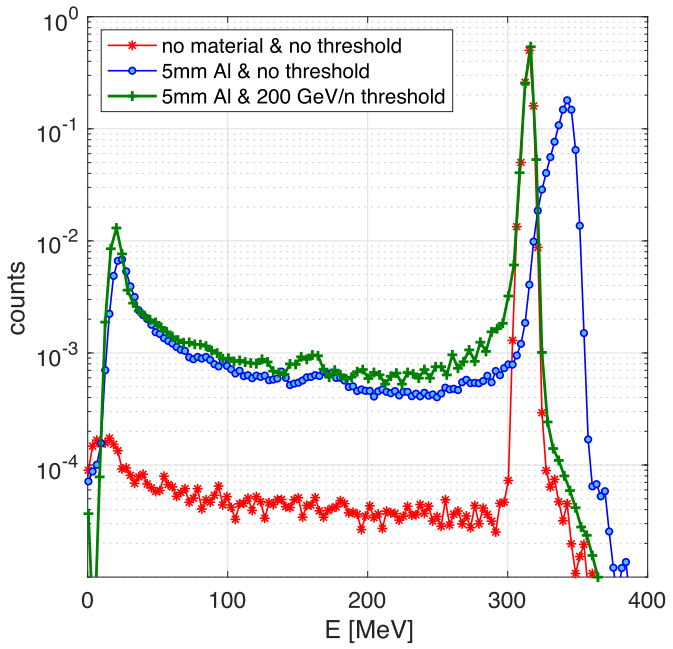

Fig. 5. FLUKA simulation of the energy deposition spectra in a 140-μm silicon detector for 150-GeV/n ^{208}Pb.

The main peak in Fig. 3, caused by direct ionization of the ^{208}Pb beam, occurs at a higher energy and is broader when aluminum is directly attached in front of the SV. This phenomenon can be explained by the energy deposition of secondary high-energy electrons (referred to as delta-rays) produced by interaction of the primary beam with the material directly in front of silicon. A proof of this explanation can be retrieved from Fig. 5.

In Fig. 5, the same 140-μm silicon diode has been simulated, applying a 150-GeV/n ^{208}Pb beam as in Fig. 3. Now, three cases are shown: First, in red, the simulation without any material or changes in the physics, second in blue 5 mm

of aluminum directly applied at silicon, and third in green 5 mm of aluminum directly attached at the silicon and disabled delta-ray production in the aluminum material. The peak shift disappears when the delta-ray production is disabled, whereas the curves look very similar apart from that; this shift clearly stems from the delta-ray electrons produced in aluminum and depositing their energy in silicon.

Hence, the FLUKA-simulated overall deposited energy is reasonably higher for a test situation where some material, such as aluminum, is present directly above the sensitive region, as demonstrated by the fact that the peak shift disappears when disabling the production of delta rays in the aluminum slab.

It is relevant to note that 1) the shift of the peak is similar in the 5- and 50-mm cases, meaning it is dominated by a very thin material layer immediately above the SV (as will later be quantified) and 2) when a thin air layer is placed between the aluminum slab and the diode, and as opposed to the intermediate energy deposition behavior, the shift of the peak disappears.

To understand the occurring nuclear interaction phenomena in more detail, the relationship between the different parameters involved must be considered. Therefore, the nuclear interaction happening between an impinging particle and the material can be described through (1):

$$P_{\text{int}}(x) = 1 - e^{-\frac{x}{\lambda}} = 1 - e^{-N\sigma x} \tag{1}$$

$$N = \frac{N_{\text{A}}}{\text{A}}\rho. \tag{2}$$

The distance a primary particle has traveled through the material is described by x in this equation, λ represents the inelastic interaction length, the atomic density is given by N in relation to the Avogadro number N_{A} in (2), ρ is the material density, and σ is the nuclear reaction cross section.

As described above, the number of nuclear interactions a particle experiences while traversing the material depends on various parameters linked to the material itself. Therefore, deposited energy distributions differ depending on the beam and the material in the beam line. Fig. 3 shows that the differences in the overall height of the distributions and the main peak shift are the most prominent features when the intercepting material thickness is changed. These observations can be explained using the earlier introduced nuclear interaction probability relation. Indeed, the intermediate part of the distribution is higher when more material is inserted in the beam line. Moreover, the main peak shift occurs due to the higher amount of deposited energy due to delta electrons of materials immediately above the sensitive area, as described earlier.

Comparing the measurements in Fig. 2 with the simulations in Fig. 3, the direct ionization peak location is slightly shifted. Experimentally, it is observed at approximately 250 MeV, whereas in the simulations it is expected at 314.5 MeV. This effect could be due to the impact of the preamplifier on the diode calibration and will be further investigated in the future. Indeed, the calibration factor that allows extracting the deposited energy from the collected charge was derived from an alpha source calibration in vacuum, with a 40-dB amplifier, as described in Section II-B.

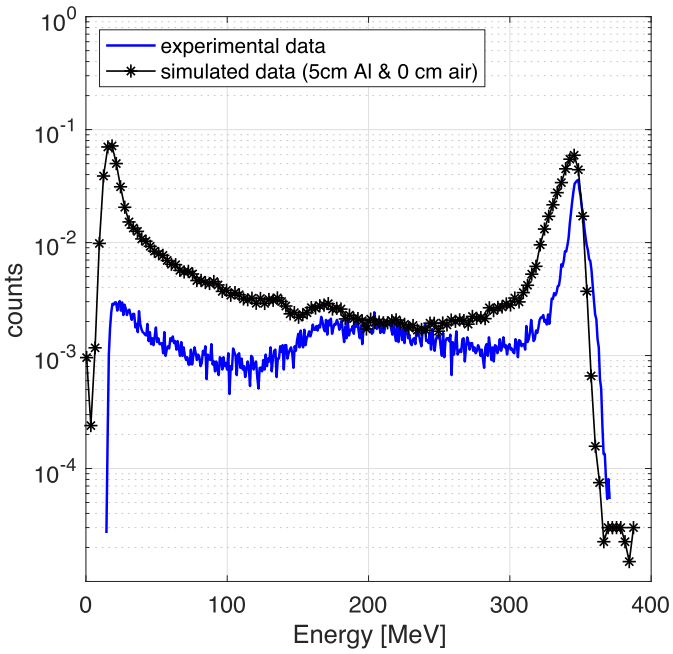

Fig. 6. FLUKA simulation of the energy deposition spectra in a 140-μm silicon detector for 150-GeV/n ^{208}Pb compared to experimentally retrieved and recalibrated data of the same beam parameters.

Furthermore, the intermediate part between 20 and 250 MeV appears to be higher in the experiment compared to the simulation without any material in front of the detector in Fig. 3. This is likely due to the inserted material in the beam line, which increases the number of secondary particles and inelastic fragments in front of the SV originated from interaction between the primary beam and the material present in the beam line. Therefore, the ratio between the intermediate part (approximately 50–300 MeV) and the direct ionization peak fits the best between simulation and experiment for the simulation case of 5-cm aluminum in front of the SV. In the experimental data, this ratio is roughly 15 and in this specific simulation it is roughly 18. In Fig. 6, the experimental data retrieved in a 150-GeV/n ^{208}Pb beam during the test campaign at CERN 2018 (blue curve) is compared to the simulation of the same beam parameters on 5-cm Al directly attached in front of the SV of 140-μm silicon (black curve). The experimental curve has been recalibrated using the energy deposition peak of the simulations. The differences occurring between simulation and experiment in this region are caused by the lack of knowledge concerning the exact composition, position, and amount of the material in the beam line in front of the detector during the experiment (other experimental setups, beam instruments, etc.).

Nevertheless, the shape remains consistent between simulations and experiments: a smaller peak in the beginning, followed by an intermediate continuum of deposited energy from fragments caused by the material present in the beam line, until the main direct ionization peak occurs.

It is to be noted that a deposited energy of 314.5 MeV in 140 μm corresponds to a volume-equivalent LET of 9.75 MeV cm^2/mg, whereas the unrestricted LET value for a 150-GeV/n ^{208}Pb beam in silicon is 15.7 MeV cm^2/mg. These

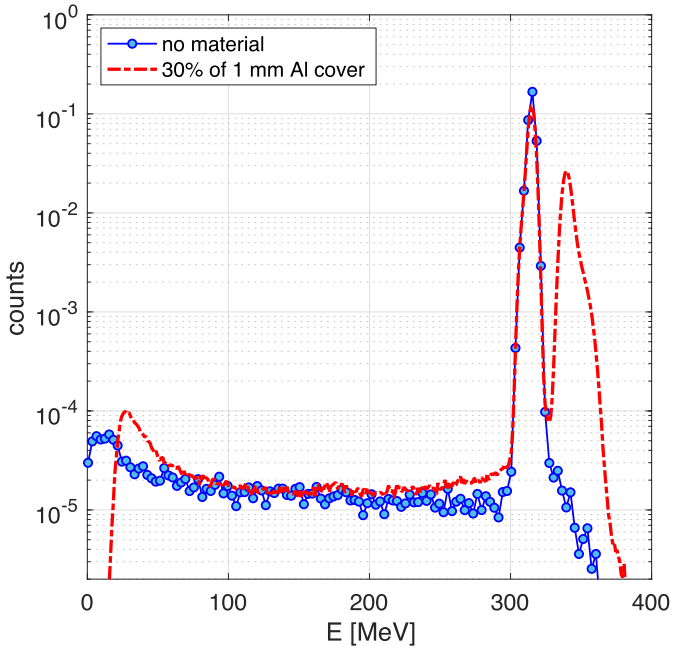

Fig. 7. FLUKA simulation of the energy deposition spectra in a 140-μm silicon detector for 150-GeV/n ^{208}Pb. 1-mm aluminum has been placed in front of the SV covering 30% of the SV area.

values have been derived via Monte Carlo simulations, which have been performed with FLUKA, as will be discussed later.

Moreover, we remind that the higher direct ionization peak is only observable when the material is directly attached to the SV. As soon as air is introduced between the material and the SV, as seen in Fig. 3, the peak shift disappears but the stronger continuum remains. While secondary electrons created in aluminum contributing to the direct ionization peak shift are absorbed by a relatively short distance in air, inelastic fragments can reach the SV unperturbed.

As mentioned above, the impact of the forwardly directed delta rays in the peak shift introduced by Al was also confirmed through simulations. This was done by disabling the delta-ray production in aluminum and confirmed the observed shift.

As a further illustration of the secondary electron effect, an aluminum slab covering 30% of the SV surface was simulated in the center of the beam and directly attached in front of the detector. The resulting energy deposition distribution in Fig. 7 shows that, in addition to the direct ionization main peak at 314.5 MeV, there is a second, clearly separated, peak at 340 MeV.

As can be seen, the partly covered SV causes the lead ions to deposit their energy in the main direct ionization peak at 314.5 MeV and, on the other hand, delta-ray electrons are also depositing an additional amount of energy in the SV for the fraction of diode covered with aluminum. Hence, the way the device packaging is designed might play an important role in the resulting energy deposition and SEE phenomena. This has also been observed and studied by several groups, among others in the work of Bagatin *et al.* [38] and Turflinger *et al.* [39].

B. LET and Deposited Energy of UHE Heavy Ion Beams

As a next step, the relationship between the LET and the fragments involved in this process needs to be understood

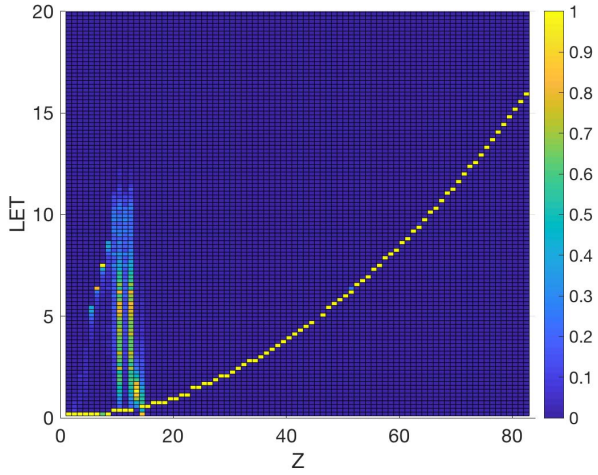

Fig. 8. FLUKA simulation of the LET spectra in a 140-μm silicon detector for 150-GeV/n ^{208}Pb without any material in front of the SV.

in more detail. For this purpose, FLUKA simulations of a 150-GeV/n ^{208}Pb beam on a 140-μm silicon detector were performed and the fragments were filtered by Z up to 82. The results of these simulations can be seen in Fig. 8. The x-axis corresponds to the atomic mass of the nuclear fragments generated in the interaction of a 150-GeV/n ^{208}Pb beam with 140 μm of silicon, whereas the y-axis is related to the nuclear reaction product LET, and the color is linked to the abundance of fragments for a given Z and LET value. The main purpose of the plot is to highlight the two different distributions that arise as nuclear reaction products. The first is the one with a Z value around 14 (that of the target material, silicon) and an LET distribution reaching relatively large values of $\sim$10 MeV cm^2/mg for the target-like fragments, thus near their energy deposition Bragg peak, highlighting their relatively low energy. In contrast, the second distribution, extending up to the projectile Z value, corresponds to the projectile-like fragments, with energies per nucleon similar to those of the projectile itself, as further shown and discussed in [17].

It is to be noted that for the high-energy, projectile-like fragments, the energy deposition in micrometric volumes can be considered proportional to the LET, which is not the case for low-energy fragments, which can stop in distances smaller than the SV dimensions.

IV. LET Dependence With Energy and SV Thickness

It is a general practice in space engineering not only to minimize the size and weight while optimizing the costs, but also to make sure that the sensitive devices are placed strategically in the best possible position to avoid radiation damage via total ionizing dose (TID). This means that the sensitive devices will be surrounded by other materials that contain less sensitive parts for protection [40]. Unfortunately, when it comes to UHE heavy ions, the interaction between the shielding material, device packaging, or any material present between the particle and the SV leads to fragmentation. Therefore, the interactions between the very energetic ion and the material need to be taken into account when looking at SEE rates and protection of a device [10], [38].

Moreover, these energies are present in the GCR environment, to which space applications are exposed.

It is relevant to stress the fact that as opposed to lower energy particles (with higher LET), the relative energy loss occurring, when a UHE particle of 150 GeV/n traverses several millimeters or even centimeters of aluminum, is negligible. The particle energy remains constant in this case and therefore the change in the volume-equivalent LET is not connected to the change in energy. The unrestricted particle LET is constant. As an example, a calculation of the deposited energy in aluminum for 150-GeV/n ^{208}Pb with an unrestricted LET of 15.7 MeV cm^2/mg on 2-mm aluminum with a density of 2.7 g/cm^3 (which is the maximum thickness used in this article) shows that the lost energy in aluminum is approximately 0.3% of the total energy. Therefore, the relative energy loss in aluminum can be regarded as negligible. However, even if the energy loss of the primary particle is low, due to its low LET, the interaction with the material and the energy deposited by the resulting secondaries with a lower LET needs to be considered.

Hence, with the purpose of placing the results above in the context of implications on SEE induction, this section focuses on the following aspects.

1) The effects of the packaging material on the volume-equivalent LET in the SV.
2) The relationship between volume-equivalent LET and kinetic energy of the primary beam.
3) The potential influence of the SV size on the LET.

A. Impact of Energy

Previous studies [41]–[43] focused on the radial distribution of an incident particle in the material showed that the energy deposition is highly concentrated in the vicinity of the trajectory of the primary particle. The kinetic energy and therefore the velocity of these particles play a relevant role with regard to the maximum energy deposited by the delta electrons.

Fig. 9 shows the correlation between the volume-equivalent LET as a function of the kinetic energy of the primary beam for a 140-μm silicon detector for the case of 1-mm aluminum and no material in the beam. A difference in LET for the two simulation setups is observable. For all cases including 1 mm of Al in front of the diode, the LET is higher than without material in the beam line, regardless of the particle energy.

The relationship between the volume-equivalent LET and aluminum thickness is detailed in Fig. 10. There the volume-equivalent LET is illustrated as a function of aluminum thickness for a 150-GeV/n ^{208}Pb beam up to 2 mm. A fast increase in the volume-equivalent LET is visible for thicknesses below 10 mm. Furthermore, the differences in LET are even more pronounced for thicknesses below 0.1 mm, whereas a saturation LET value of 10.34 MeV cm^2/mg is reached at 0.8 mm, which remains mostly stable (for 20 mm with 10.36 MeV cm^2/mg). Therefore, the main LET change happens already at thicknesses below 0.8 mm. The inserted subplot in Fig. 10 emphasizes the steep increase in LET specifically in the region below 0.2 mm.

This shows that even small differences in the material thickness in front of a detector, in this case aluminum, can have an influence on the deposited energy and hence the volume-equivalent LET. This leads to the conclusion that packaging and surrounding of a device can have a strong influence on the deposited energy in the SV, in the case of relatively large volumes, as that of the considered 2 mm $\times$ 2 mm $\times$ 140 μm diode.

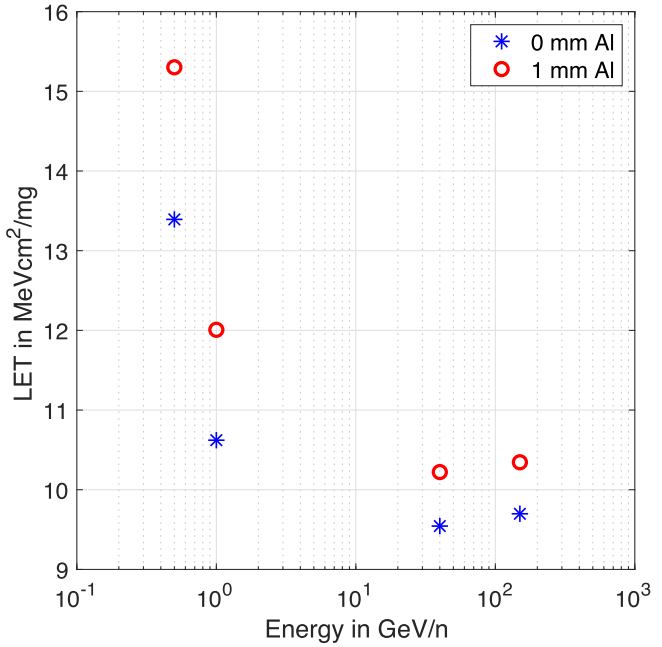

Fig. 9. Volume-equivalent LET distribution with respect to the kinetic energy of the primary particle. Performed using FLUKA simulations of ^{208}Pb for different energies varying between 500 MeV/n and 150 GeV/n in a 140-μm silicon detector. In red with a 1-mm Al layer directly in front of the SV and in blue without.

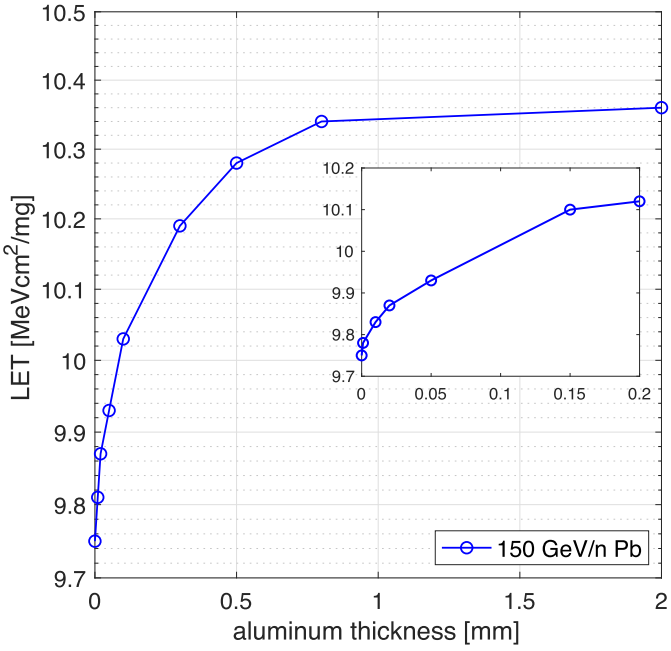

Fig. 10. LET distribution in relation to Al thickness (in mm) present directly in front of the SV up to 2 mm. The small inserted plot represents a zoom and shows the LET for Al up to 0.2-mm thickness. Performed using FLUKA simulations of 150-GeV/n ^{208}Pb in a 140-μm silicon detector.

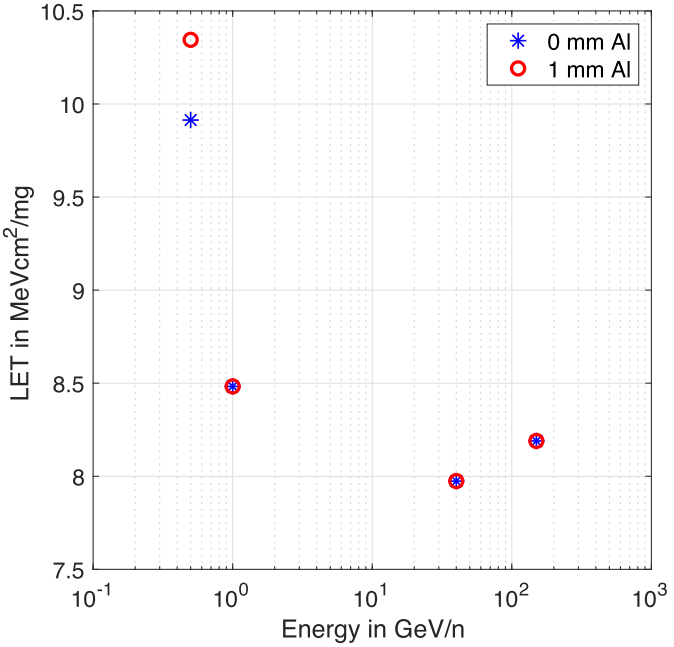

Fig. 11. Volume-equivalent LET distribution with respect to the kinetic energy of the primary particle, performed using FLUKA simulations of ^{208}Pb for different energies varying between 500 MeV/n and 150 GeV/n in an SEU detector with 100 SV of 1 μm^3. In red with a 1-mm Al layer directly in front of the SV and in blue without.

B. Impact of SV Geometry

As a second part of the study on the LET, the influence of the SV thickness is analyzed. As opposed to the 140-μm SV size used before in Section IV-B, a volume with a cubic SV size of 1 μm^3, which is representative of charge collection dimensions for single-event upsets (SEUs), has now been simulated and exposed to the same ^{208}Pb beam conditions as described in Section IV-A. The resulting LET over the primary particle kinetic energy can be seen in Fig. 11.

In this case, the impact of the 1-mm aluminum on top of the SV is negligible for energies above 0.5 GeV/n. As we will later show, this is mainly linked to the geometrical development of the ionization column as the ion travels through matter. Furthermore, an interesting observation is that for 0.5 GeV/n, the difference between the LET with and without 1 mm of aluminum in the beam line is significant, as it was for the larger SV in Fig. 9. The reason for this is the energy loss occurring in the 1 mm of Al and the resulting higher LET. As discussed above, this effect is negligible for more energetic beams.

To further evaluate the evolution of the energy deposition of UHE ion beams in silicon, simulations consisting of an incident pencil ion beam impinging in the center of a 2 $\times$ 2 mm^2 silicon structure are performed.

The total depth of silicon is set to 560 μm, and, therefore, corresponding to four times the size of the diode. The delta-ray threshold and electron production and transport energy thresholds are set to the minimum possible FLUKA value of 1 keV. The beam travels from left to right, starting at a radial position $r = 0$. The resulting dose distribution in a 2-D cylindrical scoring projection can be seen in Fig. 12.

It can be observed that there is an energy deposition build-up effect as the ion travels through silicon. The evolution

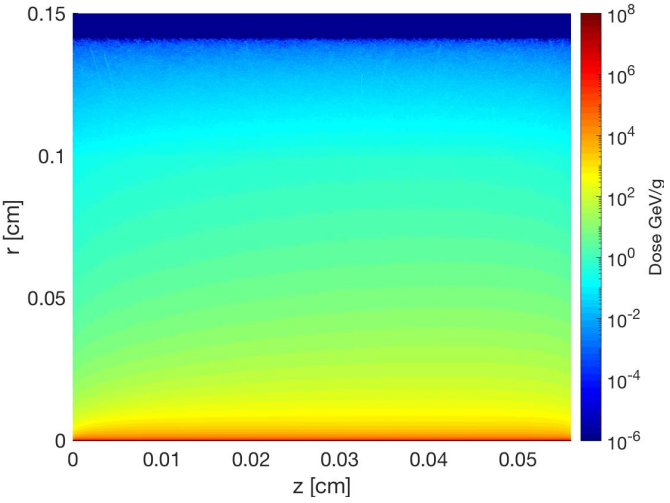

Fig. 12. 2-D illustration of performed FLUKA energy deposition simulation of UHE ion in silicon.

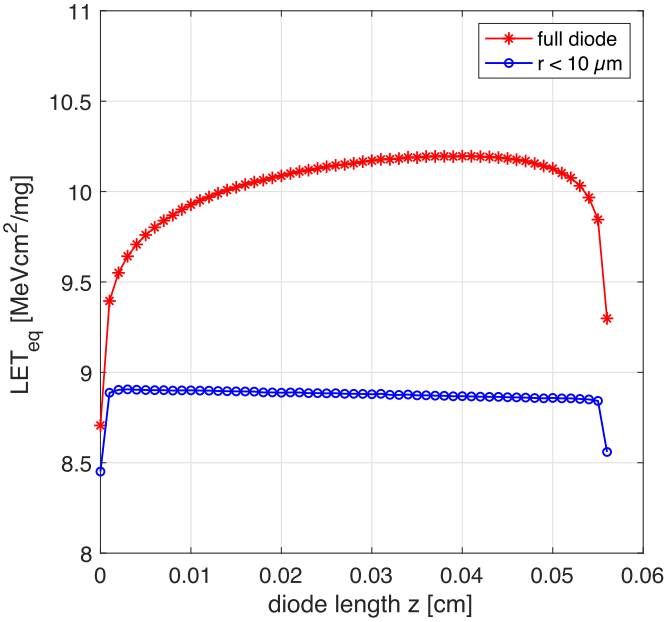

Fig. 13. FLUKA simulation of the volume-equivalent LET over the diode length z of a 150-GeV/n Pb beam in silicon, both for the full diode and a radius of 10 μm around the beam trajectory.

can be further quantified by projecting the 2-D cylindrical scoring of the dose on the z-axis as a 1-D plot and converting the dose into the volume-equivalent LET. This is done both for the full diode and a track of 10-μm radius around the ion trajectory in Fig. 13.

As can be seen in Fig. 14, the maximum volume-equivalent LET for the full 2 $\times$ 2 mm^2 geometry is roughly 10.2 MeV cm^2/mg (a factor of 1.17 with respect to the value in the first micrometer, corresponding to 8.7 MeV cm^2/mg) and it is reached at around 400-μm depth. However, for the 10-μm radius, the value is roughly constant at 8.7 MeV cm^2/mg and it reaches this value (only a factor of 1.03 larger than the first micrometer value) at a depth of roughly 10 μm.

In other words, the delta-ray build-up effect, as shown in Fig. 13, mainly impacts the region several tens of micrometers away from the beam trajectory. Therefore, although

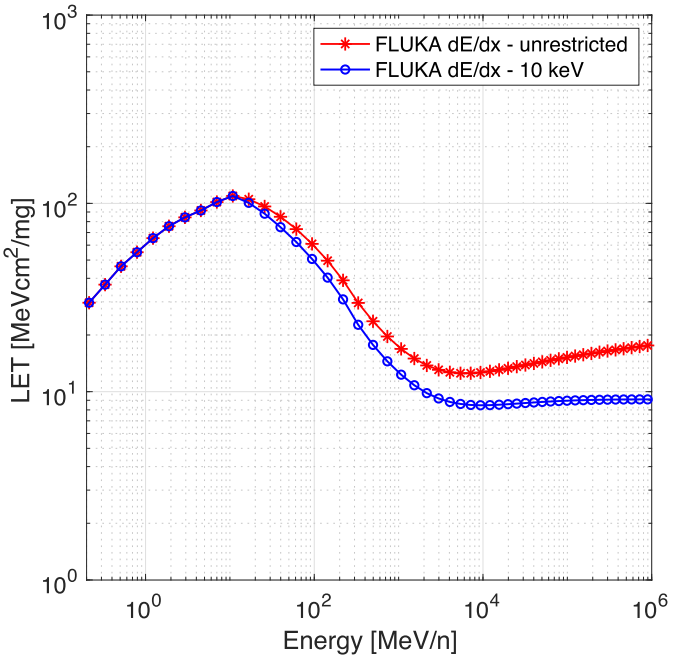

Fig. 14. Comparison of the resulting particle LET simulated using FLUKA and correlated with the deposited energy in the SV for the unrestricted and 10-keV restricted case.

relatively broad structures, such as the silicon diode, are impacted in terms of volume-equivalent LET, this will not be the case for smaller, SEU-like volumes.

However, it is worth noting that the volume-equivalent LET in the region of radius between 10 and 20 μm from the ion trajectory is 0.2 MeV cm^2/mg and could, therefore, lead to delta-ray-induced SEUs in components with very low LET thresholds (e.g., sensitive to direct proton ionization) and potentially impacting multiple cells.

Finally, Fig. 14 compares the FLUKA LET values in the unrestricted and 10-keV restricted cases. The restricted LET is defined as the energy lost by the ion through electrons (i.e., delta rays) up to a given energy. If this limit is set to 10 keV (corresponding to an electron range of 1.5 μm according to the NIST ESTAR value [44]), energy deposition from delta rays above this energy is not considered, and, therefore, restricting the value to energy that is deposited near ($\sim$1.5 μm) the track of the ion.

For 150 GeV/n, the LET restricted to 10 keV is 9.0 MeV cm^2/mg, whereas the unrestricted one reaches a value of 15.7 MeV cm^2/mg. Therefore, this implies that the energy deposited in the relatively large detector structure is still significantly below the energy actually lost by the ion, meaning that a nonnegligible fraction still escapes from the structure. It is also worth highlighting that both curves start to diverge at an energy near 100 MeV/n.

V. Discussion and Radiation Hardness Assurance Implications

In [4], it was concluded that for energies above $\sim$1 GeV/n, the volume-equivalent LET starts to diverge from the tabulated, unrestricted values for a 1-μm^3 volume, mainly owing to the radial profile of the energy deposition distribution being larger than the collection volume dimensions.

In this article, we perform a similar study focusing on the impact of the material placed directly above the SV, as is practiced under experimental condition (e.g., packages, etc.). The simulation results show that the material placed directly above an SV of 140 μm (sensitive thickness of the diode) will cause a nonnegligible increase in the direct ionization energy deposition peak (e.g., by $\sim$13% for 150-GeV/n ^{208}Pb on 1 mm of aluminum), however this is not the case for SEU-like, micrometric volumes, for which the volume-equivalent LET is unaltered by the additional material.

However, the impact of the produced fragments within the beam line on SEE testing should be kept in mind, as has been shown in this article and earlier by Kastriotou *et al.* [10]. There, it was observed that fragments had a different contribution to the beam composition, depending on the primary particle beam energy. Fragments originated from UHE or VHE heavy ion beams have a similar energy per nucleon when compared to the primary ion beam, but they have a lower LET due to their lower Z.

VI. Conclusion

Performing SEE tests with very high (1–5 GeV/n) and ultrahigh (5–150 GeV/n) energies is attractive due to their very high penetration depth, enabling accessibility to the sensitive areas of complex components in air and without the need of un-packaging the parts. Since these energies are present in the GCR environment, they are of interest for in-orbit high-energy GCR energy deposition profiles, as opposed to the lower energy standard test opportunities. These energies are becoming even more relevant with regard to the increasing complexity and 3-D stacked devices and heat shields on the die surface because they promise testing without decapsulation. To ensure an efficient testing and proper postprocessing of the retrieved data, interactions between UHE heavy ion beams and the material must be investigated to a certain degree, notably linked to the energy deposition enhancement originated from the interaction between the primary ion with different material of each surface layer.

Moreover, it is important to carefully characterize the nature of the interactions of such beams with matter, and their implications on SEE testing. For such purpose, the use of solid-state detectors, that is, the silicon diode presented in this article, is highly relevant as they provide not only a binary output of whether an SEE occurs, but also the actual energy deposition distribution in the device.

The experimental and simulated results shown in this article highlight two important features of UHE beams and their use for SEE testing.

1) Significant beam fragmentation occurs, leading to a lower amount of energy deposition (or volume-equivalent LET) events than the primary beam.
2) Secondary electrons from materials directly in contact with the SV can lead to an enhanced energy deposition for SV characteristic sizes in the order of 100 μm.

It is important to note that the relevant particles leading to effect 1 are highly penetrating, due to the increasing absolute impact proportional to the material thickness present in the

beam line (produced fragments are not stopped in several centimeters of air), whereas effect 2 is only relevant for cases in which the material is placed directly above the SV.

REFERENCES

[1] A. Virtanen, R. Harboe-Sorensen, A. Javanainen, H. Kettunen, H. Koivisto, and I. Riihimaki, "Upgrades for the RADEF facility," in *Proc. IEEE Radiat. Effects Data Workshop*, Honolulu, HI, USA, Jul. 2007, pp. 38–41, doi: 10.1109/REDW.2007.4342538.

[2] *Centre du Recherches du Cyclotron Universit Catholique de Louvain-la-Neuve*. Accessed: May 9, 2019. [Online]. Available: https://uclouvain.be/en/

[3] *Texas A&M University Cyclotron Institute Radiation Effects Facility*. Accessed: Dec. 11, 2019. [Online]. Available: https://cyclotron.tamu.edu/ref/

[4] *Berkeley Accelerator Space Effects—Lawrence Berkeley National Laboratory*. Accessed: Dec. 11, 2019. [Online]. Available: http://cyclotron.lbl.gov/base-rad-effects

[5] *KVI—Center for Advanced Radiation Technology*. Accessed: Dec. 11, 2019. [Online]. Available: http://www.rug.nl/kvi-cart

[6] M.-H. Moscatello, A. Dubois, and X. Ledoux, "Industrial applications with GANIL SPIRAL2 facility," in *Proc. 16th Eur. Conf. Radiat. Effects Compon. Syst. (RADECS)*, Bremen, Germany, Sep. 2016, Art. no. G9, doi: 10.1109/RADECS.2016.8093164.

[7] *GSI Helmholtzzentrum für Schwerionenforschung GmbH*. Accessed: Jan. 28, 2020. [Online]. Available: https://www.gsi.de/en/researchaccelerators.htm

[8] *NASA Space Radiation Laboratory At Brookhaven*. Accessed: Jan. 28, 2020. [Online]. Available: https://www.bnl.gov/nsrl/

[9] M. Stocker *et al.*, "Status of the PSI/ETH compact AMS facility," *Nucl. Instrum. Meth. Phys. Res. B, Beam Interact. Mater. At.*, vols. 223–224, pp. 104–108, Aug. 2004, doi: 10.1016/j.nimb.2004.04.024.

[10] M. Kastriotou *et al.*, "Single event effect testing with ultrahigh energy heavy ion beams," *IEEE Trans. Nucl. Sci.*, vol. 67, no. 1, pp. 63–70, Jan. 2020, doi: 10.1109/TNS.2019.2961801.

[11] P. Fernández-Martínez *et al.*, "SEE tests with ultra energetic Xe ion beam in the CHARM facility at CERN," *IEEE Trans. Nucl. Sci.*, vol. 66, no. 7, pp. 1523–1531, Jul. 2019, doi: 10.1109/TNS.2019.2907112.

[12] R. G. Alia *et al.*, "Ultraenergetic heavy-ion beams in the CERN accelerator complex for radiation effects testing," *IEEE Trans. Nucl. Sci.*, vol. 66, no. 1, pp. 458–465, Jan. 2019, doi: 10.1109/TNS.2018.2883501.

[13] E. Petersen, *Single Event Effects in Aerospace*. Hoboken, NJ, USA: Wiley, 2011.

[14] K. M. Warren *et al.*, "The contribution of nuclear reactions to heavy ion single event upset cross-section measurements in a high-density SEU hardened SRAM," *IEEE Trans. Nucl. Sci.*, vol. 52, no. 6, pp. 2125–2131, Dec. 2005, doi: 10.1109/TNS.2005.860677.

[15] T. L. Criswell, P. R. Measel, and K. L. Wahlin, "Single event upset testing with relativistic heavy ions," *IEEE Trans. Nucl. Sci.*, vol. NS-31, no. 6, pp. 1559–1561, Dec. 1984, doi: 10.1109/TNS.1984.4333548.

[16] S. K. Hoeffgen *et al.*, "Investigations of single event effects with heavy ions of energies up to 1.5 GeV/n," *IEEE Trans. Nucl. Sci.*, vol. 59, no. 4, pp. 1161–1166, Aug. 2012, doi: 10.1109/TNS.2012.2201502.

[17] V. Wyrwoll *et al.*, "Heavy ion nuclear reaction impact on SEE testing: From standard to ultra-high energies," *IEEE Trans. Nucl. Sci.*, early access, Feb. 12, 2020, doi: 10.1109/TNS.2020.2973591.

[18] P. E. Dodd *et al.*, "Impact of heavy ion energy and nuclear interactions on single-event upset and latchup in integrated circuits," *IEEE Trans. Nucl. Sci.*, vol. 54, no. 6, pp. 2303–2311, Dec. 2007, doi: 10.1109/TNS.2007.909844.

[19] R. Koga, S. H. Crain, W. R. Crain, K. B. Crawford, and S. J. Hansel, "Comparative SEU sensitivities to relativistic heavy ions," *IEEE Trans. Nucl. Sci.*, vol. 45, no. 6, pp. 2475–2482, Dec. 1998, doi: 10.1109/23.736488.

[20] *Heavy Ion Cocktails Available At RADEF*. Accessed: Jun. 25, 2019. [Online]. Available: https://www.jyu.fi/science/en/physics/research/infrastructures/accelerator-laboratory/radiation-effects-facility/heavy-ion-cocktail-1/heavy-ion-cocktails-available-at-radef

[21] *Single Event Effects Test Method and Guidelines*, Doc. 25100, ESCC Basic Specification, European Space Agency, 2014, no. 2.

[22] B. D. Reddell *et al.*, "Compendium of single event effects test results for commercial-off-the-shelf and standard electronics for low earth orbit and deep space applications," in *Proc. IEEE Radiat. Effects Data Workshop*, New Orleans, LA, USA, Jul. 2017, pp. 57–66, doi: 10.1109/NSREC.2017.8115433.

[23] S. M. Guertin and M. Cui, "SEE test results for the snapdragon 820," in *Proc. IEEE Radiat. Effects Data Workshop*, New Orleans, LA, USA, Jul. 2017, pp. 155–161, doi: 10.1109/NSREC.2017.8115452.

[24] C. Cazzaniga *et al.*, "A diamond based neutron spectrometer for diagnostics of deuterium-tritium fusion plasmas," *Rev. Sci. Instrum.*, vol. 85, no. 11, Jul. 2014, Art. no. 11E101.

[25] C. Cazzaniga *et al.*, "Single crystal diamond detector measurements of deuterium-deuterium and deuterium-tritium neutrons in joint European torus fusion plasmas," *Rev. Sci. Instr.*, vol. 85, no. 11, Apr. 2014, Art. no. 11E101, doi: 10.1063/1.4870584.

[26] G. Battistoni *et al.*, "Overview of the FLUKA code," *Ann. Nucl. Energy*, vol. 82, pp. 10–18, Aug. 2015, doi: 10.1016/j.anucene.2014.11.007.

[27] A. Coronetti, R. G. Alía, and C. Cazzaniga, "CNA low-energy protons RADSAGA campaign," CERN EDMS 2215710 V.1, Geneva, Switzerland, RADSAGA Test Rep. 07, 2019. [Online]. Available: https://edms.cern.ch/document/2215710/1

[28] A. Fasso *et al.*, "The physics models of FLUKA: Status and recent development," 2003, *arXiv:hep-ph/0306267*. [Online]. Available: https://arxiv.org/abs/hep-ph/0306267

[29] A. Ferrari, P. R. Sala, A. Fasso, and J. Ranft, "FLUKA: A multi-particle transport code," Program Version, CERN, Geneva, Switzerland, Tech. Rep. INFN-TC-05-11, 2005.

[30] R. A. Reed *et al.*, "Physical processes and applications of the Monte Carlo radiative energy deposition (MRED) code," *IEEE Trans. Nucl. Sci.*, vol. 62, no. 4, pp. 1441–1461, Aug. 2015, doi: 10.1109/TNS.2015.2454446.

[31] R. A. Reed *et al.*, "Anthology of the development of radiation transport tools as applied to single event effects," *IEEE Trans. Nucl. Sci.*, vol. 60, no. 3, pp. 1876–1911, Jun. 2013, doi: 10.1109/TNS.2013.2262101.

[32] F. Cerutti *et al.*, "New results in comprehensive calculations of heavy-ion interactions," in *Proc. AIP Conf.*, 2005, vol. 769, no. 1, pp. 1176–1179, doi: 10.1063/1.1945217.

[33] H. H. Braun, A. Fassò, A. Ferrari, J. M. Jowett, P. R. Sala, and G. I. Smirnov, "Hadronic and electromagnetic fragmentation of ultra-relativistic heavy ions at LHC," *Phys. Rev. Special Topics-Accel. Beams*, vol. 17, no. 2, Feb. 2014, Art. no. 021006, doi: 10.1103/PhysRevSTAB.17.021006.

[34] R. G. Alía, "Radiation fields in high energy accelerators and their impact on single event effects," Ph.D. dissertation, Institut d'Electronique du Sud, Université de Montpellier, Montpellier, France, 2014. [Online]. Available: https://cds.cern.ch/record/2012360?ln=es

[35] S. Roesler, R. Engel, and J. Ranft, "The Monte Carlo event generator DPMJET-III," in *Advanced Monte Carlo for Radiation Physics, Particle Transport Simulation and Applications*, A. Kling, F. J. C. Barao, M. Nakagawa, L. Tavora, and P. Vaz, Eds. Berlin, Germany: Springer, 2001, pp. 1033–1038.

[36] H. Sorge, H. Stöcker, and W. Greiner, "Poincaré invariant Hamiltonian dynamics: Modelling multi-hadronic interactions in a phase space approach," *Ann. Phys.*, vol. 192, no. 2, pp. 266–306, Jun. 1989, doi: 10.1016/0003-4916(89)90136-X.

[37] F. Cerutti *et al.*, "Low energy nucleus–nucleus reactions: The BME approach and its interface with FLUKA," in *Proc. 11th Int. Conf. Nucl. Reaction Mech.*, Varenna, Italy, Jun. 2006, pp. 1–8. [Online]. Available: http://www0.mi.infn.it/~gadioli/Varenna2006/Proceedings/Cerutti_F.pdf

[38] M. Bagatin *et al.*, "Characterizing high-energy ion beams with PIPS detectors," *IEEE Trans. Nucl. Sci.*, early access, Dec. 10, 2019, doi: 10.1109/TNS.2019.2958746.

[39] T. L. Turflinger *et al.*, "Proton on metal fission environments in an IC package: An RHA evaluation method," *IEEE Trans. Nucl. Sci.*, vol. 64, no. 1, pp. 309–316, Nov. 2016, doi: 10.1109/TNS.2016.2626960.

[40] *Calculation of Radiation and Its Effects and Margin Policy Handbook*, Standard ECSS-E-HB-10-12A, ECSS Secretariat, Dec. 2010. [Online]. Available: http://escies.org/ftp/ecss.nl/Handbooks/ECSS-E-HB-10-12A(17December2010).pdf

[41] A. Javanainen, "Particle radiation in microelectronics," Ph.D. dissertation, Dept. Phys., Univ. Jyväskylä, Jyväskylä, Finland, 2012. [Online]. Available: https://www.jyu.fi/static/fysiikka/vaitoskirjat/2012/Javanainen-Arto-2012.pdf

[42] I. Plante and F. A. Cucinotta, "Ionization and excitation cross sections for the interaction of HZE particles in liquid water and application to Monte Carlo simulation of radiation tracks," *New J. Phys.*, vol. 10, no. 12, Dec. 2008, Art. no. 125020, doi: 10.1088/1367-2630/10/12/125020.

[43] M. P. King *et al.*, "The impact of delta-rays on single-event upsets in highly scaled SOI SRAMs," *IEEE Trans. Nucl. Sci.*, vol. 57, no. 6, pp. 3169–3175, Dec. 2010, doi: 10.1109/TNS.2010.2085019.

[44] *NIST ESTAR*. Accessed: Aug. 2019. [Online]. Available: https://physics.nist.gov/PhysRefData/Star/Text/ESTAR.html